Modeling the radiative, thermal and chemical microenvironment of 3D scanned corals

Swathi Murthy[1], Cristian Picioreanu[2], and Michael Kühl[1]

[1]Marine Biology Section, Department of Biology, University of Copenhagen, Strandpromenaden 5, 3000 Helsingør, Denmark.

[2]Biological and Environmental Sciences and Engineering Division, King Abdullah University of Science and Technology, Thuwal 23955-6900, Saudi Arabia.

Abstract

1: Reef building corals are efficient biological collectors of solar radiation and consist of a thin stratified tissue layer spread over a light scattering calcium carbonate skeleton surface that together construct complex three dimensional (3D) colony structures forming the foundation of coral reefs. They exhibit a vast diversity of structural forms to maximize photosynthesis of their dinoflagellate endosymbionts (Symbiodiniaceae), while simultaneously minimizing photodamage. The symbiosis takes place in the presence of dynamic gradients of light, temperature and chemical species that are affected by the interaction of incident irradiance and water flow with the coral colony.

2: We developed a multiphysics modelling approach to simulate microscale spatial distribution of light, temperature and O_2 in coral fragments with accurate morphology determined by 3D scanning techniques.

3: Model results compared well with spatial measurements of light, O_2 and temperature under similar flow and light conditions. The model enabled us to infer the effect of coral morphology and light scattering in tissue and skeleton on the internal light environment experienced by the endosymbionts, as well as the combined contribution of light, water flow and ciliary movement on O_2 and temperature distributions in the coral.

4: The multiphysics modeling approach is general enough to enable simulation of external and internal light, O_2 and temperature microenvironments in 3D scanned coral species with varying degrees of branching and morphology under different environmental conditions. This approach is also relevant for simulating structure-function relationships in other benthic systems such as photosynthetic biofilms and aquatic plant tissue, and can also be adapted to other sessile organisms such as symbiont-bearing giant clams, ascidians, jellyfish or foraminifera. The model could also be useful in more applied research such as optimization of 3D bioprinted constructs where different designs can be evaluated and optimized.

Keywords

heat transfer; light; mass transfer; microenvironment; numerical simulation;

1. Introduction

Reef building, scleractinic corals construct a complex three dimensional (3D) calcium carbonate skeleton, which is the framework for coral reef ecosystems of considerable biological and socio-economic importance (Costanza et al., 2014). Tropical, scleractinic corals rely on endosymbiotic dinoflagellate algae from the family Symbiodiniaceae, which are hosted in the coral endoderm tissue and excrete photosynthates to the host, providing the majority (up to >90%) of carbon needed for coral animal respiration along with O_2 (Muscatine, 1973). Symbiont photosynthesis can also enhance coral calcification (Chalker, 1981; Goreau et al., 1996). In exchange, the host provides the endosymbionts with a conducive and protected environment and a steady, albeit limited supply of nutrients.

However, the coral-algal symbiosis can rapidly deteriorate under environmental stress (LaJeunesse et al., 2018), (Moberg & Folke, 1999). Environmental factors related to ongoing climate change such as ocean acidification (Jackson et al., 2001; van der Zande et al., 2020), deoxygenation (Hughes et al., 2020) (Altieri et al., 2017) and warming (Hughes et al., 2017), increasingly result in severe mass bleaching and mortality of corals (Knowlton et al., 2021). Coral bleaching and mortality varies as a consequence of solar irradiation levels (Dunne & Brown, 2001; Mumby et al., 2001), local seawater temperature variation (Teneva et al., 2012), coral colony morphology (Loya et al., 2001; Van Woesik et al., 2012), water flow around the coral (Jimenez et al., 2008; Nakamura et al., 2003), and O_2 levels in the surrounding water (Altieri et al., 2017; Hughes et al., 2020; Johnson et al., 2018). Hence, it is important to improve the mechanistic understanding of how the photobiology and physiological activity of the coral holobiont are affected by macroscale colony morphology and microscale variations in tissue/skeleton

architecture, and how interactions with the incident solar irradiance and flowing seawater modulate the physico-chemical microenvironment and metabolic activity of corals. This will enable us to better estimate hotspots for coral bleaching, the coral reef's response to environmental stressors, and the relationship between the host microenvironment and microbiome/endosymbiont populations. Understanding of light propagation, heat and mass transfer in relation to the 3D morphology of a coral colony can also provide insight into the mechanisms governing spatial and temporal variability in coral bleaching and recovery within and between coral species.

Corals are efficient biological collectors of solar radiation (D. Wangpraseurt et al., 2014) and consist of a thin (from ~100 μm to several mm) stratified tissue layer spread over a light-scattering skeleton matrix (Davy et al., 2012). They are exposed to a wide range of light environments ranging from super-saturating, broadband (UV to near infrared) solar irradiance in the shallow reefs (Jimenez et al., 2012; Veal et al., 2010; Wangpraseurt et al., 2014) to very low illumination in the blue-green spectral range at mesophotic depths (Eyal et al., 2015; Tamir et al., 2019). The morphology of the colony and the surrounding reef, along with the optical properties of the host tissue and skeleton, can lead to variable light conditions experienced by different parts of a coral colony and hence the endosymbionts (Kaniewska et al., 2011; Wangpraseurt et al., 2014).

Corals have developed a vast diversity of structural forms and mechanisms at cellular, polyp and colony level, to maximize photosynthesis of their endosymbionts under spatial and temporal variation in light availability (Anthony & Hoegh-Guldberg, 2003; Kaniewska et al., 2011; Todd et al., 2008), while simultaneously minimizing photo-damage (Brodersen et al., 2014; Terán et al.,

2010) and oxidative stress (Pacherres et al., 2022), and maximizing solute and heat exchange (Jimenez et al., 2011). Consequently, corals can reach high photosynthetic quantum efficiencies close to 0.1 O_2 photon^{-1}, approaching theoretical limits, under moderate irradiance levels (Brodersen et al., 2014; Dubinsky et al., 1984).

Light absorption by corals not only drives symbiont photosynthesis *in hospite*, but can also affect the thermal microenvironment via local heating (Jimenez et al., 2008), as most of the absorbed light energy is dissipated as heat (Brodersen et al., 2014). Light is mainly absorbed in the coral tissue and, to some extent, in the skeleton by endolithic algae and photosynthetic bacteria (Kühl et al., 2008). However, both coral morphology (Kaniewska et al., 2011; Kaniewska & Sampayo, 2022; Kramer et al., 2022) and the inherent scattering properties of coral skeleton and tissue modulate light propagation and thus the light exposure of the microalgal symbionts (Enríquez et al., 2005; Wangpraseurt et al., 2016) (Bollati et al., 2022; Lyndby et al., 2016).

The morphology and the degree of branching in coral colonies affect not only the light field but also the water flow around the colonies. The flow determines the thickness and shape of boundary layers for momentum transfer (MBL, i.e., water velocity change near the coral surface), mass transfer (DBL, i.e., concentration change in the diffusion-dominated region adjacent to the coral tissue) (Chan et al., 2016), as well as heat transfer (TBL, referring to temperature changes) (Jimenez et al., 2008; Ong et al., 2019). The coral consumes part of the O_2 produced by the symbionts under light (Al-Horani et al., 2003), while an eventual surplus of oxygen and heat generated in the tissue is transported into the surrounding water column and the coral skeleton. By introducing a resistance to mass and heat transfer, boundary layers decrease the mass and heat exchange rates between the bulk water and the coral, to the extent in which solute diffusion

(Shashar et al., 1993) and heat conduction (Ong et al., 2012; Ong et al., 2017; Ong et al., 2019) can become bottlenecks. These transfer resistances can be alleviated to some extent by actively decreasing boundary layer thickness through an intensified flow, as achieved by tissue and polyp level changes like contraction-expansion and ciliary movement that can enhance mass (Pacherres et al., 2020; Pacherres, 2022; Shapiro et al., 2014) and heat (Ong et al., 2017) transfer, along with affecting light penetration (Wangpraseurt et al., 2014; Wangpraseurt et al., 2017). The resulting spatial and temporal variations in temperature distribution and concentration of chemical species (e.g., dissolved oxygen, inorganic carbon and pH) affect the coral microenvironment and can form distinct microhabitats within a given coral colony. Such fine scale ecological niche heterogeneity may affect the composition of both endosymbionts and microbiomes across the different compartments of the coral holobiont, but the microscale fitness landscape of corals remains largely unexplored, in part due to technical challenges (Hughes et al., 2022).

Numerical modelling is a powerful way to integrate the physical, chemical and biological complexity (at several spatial and temporal scales) into a systematic framework, with the aim to describe, understand and ultimately predict coral responses to a changing environment. Modelling the growth of coral colonies in response to environmental parameters has been pioneered by the work of Kaandorp and coworkers (Chindapol et al., 2013; Kaandorp, 2013). Several studies have also modeled the interaction of light and fluid flow with colony morphology and the resulting surface temperature (Ong et al., 2012; Ong et al., 2018; Ong et al., 2017; Ong et al., 2019) and mass transfer at the coral surface (Chang et al., 2014; Shapiro et al., 2014). However, these models have not included radiative transfer in the tissue-skeleton matrix, or

simulations of internal gradient of light, temperature and chemical parameters across the tissue and skeleton.

Empirical and theoretical models have shown how skeleton-dependent scattering can enhance the local light field and absorption of Symbiodiniaceae *in hospite* (Enríquez et al., 2005; Swain et al., 2016). Ray tracing (Ong et al., 2018) and probabilistic Monte Carlo (MC) modeling techniques for light propagation (Terán et al., 2010; Wangpraseurt et al., 2016) assuming a simple two-layer tissue-skeleton geometry have also been employed. Recent advances in estimating inherent optical properties of different species of living corals (Jacques et al., 2019; Spicer et al., 2019; Wangpraseurt et al., 2018) now enable more accurate simulation of internal light fields in specific corals.

We recently developed a numerical model of a stratified coral tissue on top of skeleton to link internal light distribution to light absorption, radiative heat dissipation, heat transfer and mass transfer of photosynthetically produced O_2 (Taylor Parkins et al., 2021). The model couples a Monte Carlo (MC) simulation of light propagation with numerical modelling of heat production and metabolism inside the coral to simulate irradiance, temperature and O_2 microprofiles at small scale in simplified, schematic geometries. In the present study, we have expanded this multiphysics modelling approach to simulate microscale distribution of light, temperature and O_2 in and around branched coral fragments (cm scale) with complex, natural morphology, as determined by 3D scanning techniques. We validate the model by comparing simulated microenvironmental parameters over the coral topography with the corresponding microscale measurements on the same fragment under similar irradiance and laminar flow conditions. This enabled us to describe the effect of coral morphology on the internal light environment and the

combined effects of light, water flow and ciliary movement on the O_2 and temperature distribution in the coral. The presented modeling approach can easily be adapted for simulating effects of flow and irradiance on the optical, thermal and chemical microenvironment in other types of aquatic organisms and systems with a defined structural composition, either reflecting their natural structure, as obtained from 3D scanning, or more schematic idealizations, e.g. in bionic 3D bioprinted constructs.

2. Materials and methods

The methodological approach involved an experimental and a theoretical part. First microsensor measurements of light, O_2 and temperature were performed on a fragment of the branched coral *Stylophora pistillata* (Figure 1a,b) in a flow chamber under defined irradiance and flow conditions. The fragment was subsequently 3D scanned and meshed (Figure 1c,d), followed by multiphysics 3D modeling of the radiative, heat and mass transfer of the meshed structure (Figure 1f) and subsequent comparison of simulated distributions of light, O_2 and temperature with the experimental measurements (Figure 1e).

2.1 Coral specimens and husbandry

Colonies of the branched coral *Stylophora pistillata* were obtained from a sustainable, commercial provider (Dejong Marine Life, Netherlands). Colonies were fragmented into smaller nubbins that were mounted in small plastic caps using AF Gel Fix (https://aquaforest.eu) and kept in dedicated aquaria supplied with continuous flow of artificial reef water at 25-26°C, salinity of 36 g/kg, and moderate levels of downwelling photon irradiance (150 - 200 µmol photons m^{-2} s^{-1};

400–700 nm) provided over a 12:12 hour dark-light cycle by a programmable aquarium lamp (MAXSPECT R5X 150W; Decocean Aquarium).

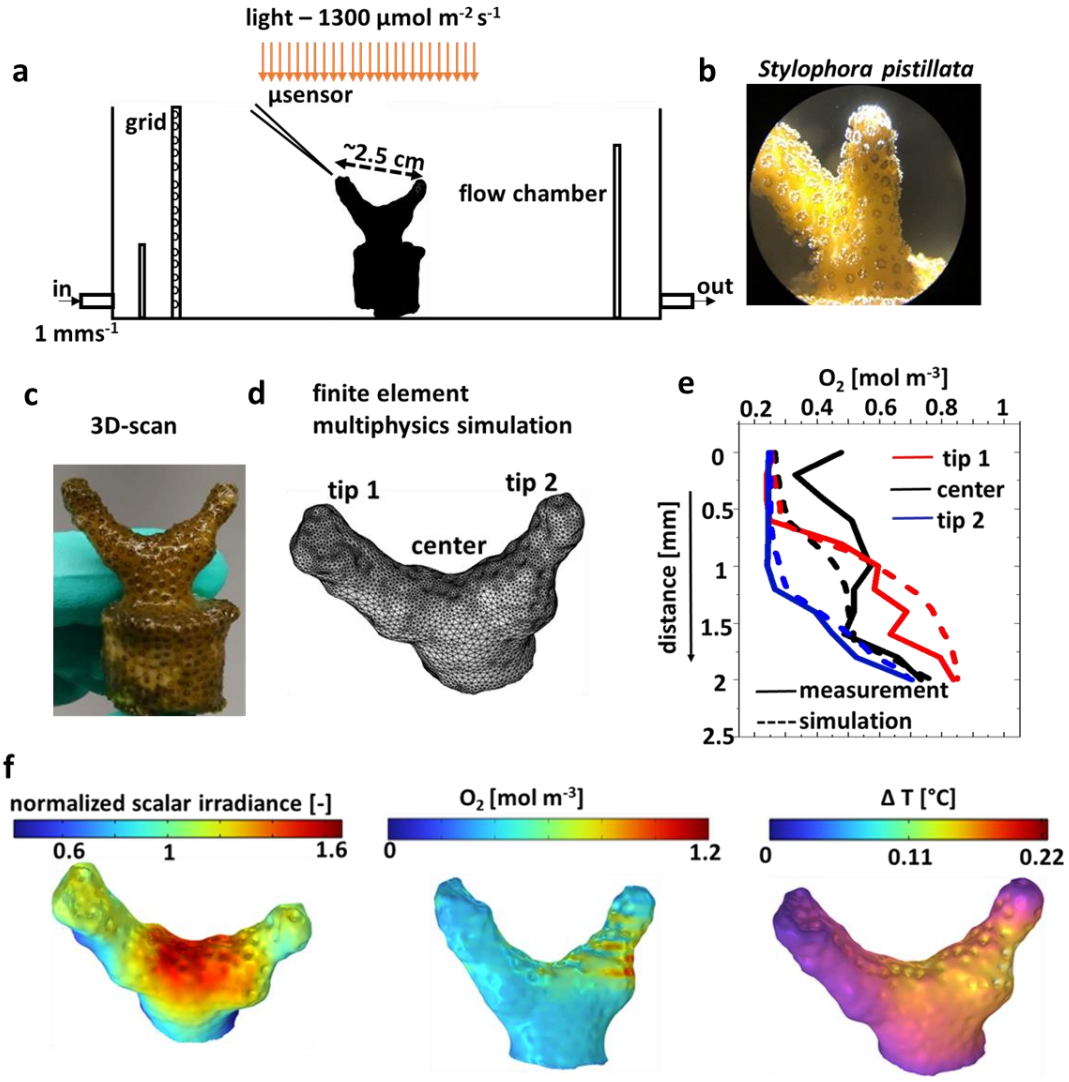

Figure 1: Overview of experimental and modeling approach. Experimental flow chamber set-up for microsensor measurements (a) on a coral fragment of *Stylophora pistilla* (b,c). Tetrahedral mesh based on the 3D scan of the coral (d), used for multi-physics simulation. Comparison of microsensor measurements and simulations (here illustrated with measured and simulated O_2 concentration profiles) in particular areas of the coral (e). Simulated surface values of normalized scalar irradiance, O_2 concentration and temperature at the coral tissue-water interface (f).

2.2 Experimental setup

A small fragment of *S. pistillata* (Figure 1b) was placed in a custom-made black, acrylic flow chamber, and measurements were done with two different orientations of the fragment relative to the laminar flow. The samples were placed for at least 1 hour in the chamber prior to microsensor measurements to ensure steady-state conditions. The coral fragment was continuously flushed with aerated seawater at 26°C and salinity of 35 g/kg. An average flow velocity of ~1 mm s^{-1} was maintained by a water pump connected to the flow chamber and submerged in the thermostated aquarium reservoir.

The sample was illuminated with a constant downwelling photon irradiance of 1300 µmol photons m^{-2} s^{-1} from a fibre-optic tungsten halogen lamp equipped with a heat filter and a collimating lens (KL-2500LCD, Schott GmbH, Germany), positioned vertically above the flow chamber (Figure 1a). The downwelling photon irradiance (E_d in units of µmol photons m^{-2} s^{-1}) of photosynthetically active radiation (PAR; 400–700 nm) was measured with a calibrated photon irradiance meter (ULM-500, Walz GmbH, Germany) equipped with a planar cosine collector (LI-192S, LiCor, USA) positioned in the light path approximately at the same distance as the coral.

2.3 Microsensor measurements

Measurements were conducted on the connective tissue, i.e., coenosarc, between individual polyps, which had a more even topography and less contractile tissue as compared to polyp tissue.

Light measurements: Spectral scalar irradiance was measured using a fibre-optic scalar irradiance microprobe with a spherical tip diameter of ~100 µm (Rickelt et al., 2016) connected to a fibre-optic spectrometer (USB 2000+, Ocean Optics, USA). The incident downwelling irradiance was measured at the same height as the coral surface by placing the light sensor in a black (non-reflective) light well under the vertically incident light in the flow chamber. All spectral scalar irradiance measurements at the coral tissue surface were normalized to the incident spectral irradiance. The results are represented as mean ± standard deviation, averaged over 12 measurement points taken close to each other in a given region of interest (as indicated by squares in Figure 2c) and for the 2 different orientations of the fragment with respect to the flow.

Oxygen measurements: Oxygen concentrations were measured with Clark-type microelectrodes (tip diameter approx. 25 µm; OX-25, Unisense A/S, Aarhus, Denmark)(Revsbech, 1989). The microsensor was connected to a pA-meter (Oxymeter, Unisense A/S) interfaced to a PC. The O_2 microsensors were linearly calibrated from sensor signal measurements in aerated and anoxic seawater at experimental temperature and salinity.

Temperature measurements: Thermocouple microsensors (tip diameter approx. 50 mm; T50, Unisense A/S) were connected to a thermocouple meter (Unisense A/S). A high precision thermometer (Testo 110, Testo AG, Germany) was used to linearly calibrate the temperature microsensor signal from readings in seawater at different temperatures.

For measurements, the microsensors were mounted on a motorized micromanipulator (MU-1, PyroScience, GmbH), which was interfaced to a PC and controlled by dedicated data acquisition software (ProFix, Pyros-Science GmbH). All measurements were made at an angle of 45° relative

to the vertically incident light beam to avoid shading. The measurements were made at the coenosarc tissue in three different regions of the coral fragment as shown in Figure 1d. The temperature profiles were represented as the temperature increase relative to the water temperature (in the free flowing region) directly above the measurement point. The O_2 and temperature profiles were measured from the water column into the coenosarc in vertical steps of 100 µm, as described previously (Jimenez et al., 2008). Scalar irradiance measurements were done by placing the sensor tip at the coral tissue surface. Positioning of microsensor tips relative to the coral tissue surface was monitored visually by observation under a dissection scope.

2.4 3D scanning and OCT imaging

We used a PC-controlled, structured light 3D scanner (Einscan-SP, Shining 3D) to generate non-texture 3D scans of coral fragments in air. A sample was placed on the turn table of the calibrated scanner. Data acquisition and processing was controlled by the system software (EXScan S_V3; Shining 3D). The brightness setting of the scanner was adjusted to avoid saturation of the camera signal. A 360° scan of the fragment was made under different orientations, to capture the complete morphology of the fragment avoiding missing faces. The different scans were aligned using the “align by feature” mode in the scanner software. A watertight mesh of the model was exported as an STL file. The fragment was scanned with and without the tissue layer to estimate an average tissue thickness, from the volume difference between the two scans. The tissue was removed by immersing the fragment in 30% hydrogen peroxide solution overnight. This procedure led to a tissue thickness estimation of ~900 µm. However, this could be an overestimate as the reconstruction software fills in holes in the scan by extrapolation, in places

where it could not scan the object correctly (e.g., due to complex shape and highly absorbing or reflective surfaces).

For an alternative determination of the coral tissue thickness, we used a 930 nm spectral domain OCT system (Ganymed II, Thorlabs, Germany) equipped with an objective lens with an effective focal length of 18 mm and a working distance of 7.5 mm (LSM02-BB; Thorlabs GmbH, Dachau, Germany) for OCT imaging of corals immersed in seawater with a maximal axial and lateral resolution in water of 5.8 µm and 8 µm, respectively (Wangpraseurt et al., 2017). Two-dimensional OCT B-scans were acquired at a fixed pixel size of 581 x 1024. The scans were used to estimate the tissue thickness, however, due to shadowing effects and uncertainties in the exact refraction index of the coral tissue, the OCT measurements underestimated tissue thickness. For the simulations, we therefore selected a tissue thickness of 650 µm, which was inbetween the values from the OCT and 3D scans.

2.5 Numerical modeling

A three-dimensional mathematical model was constructed with the aim of simulating the spatial distribution of dissolved oxygen and temperature around and within the coral, as influenced by the light transport and by the water flow. Model predictions were compared to the measured profiles of light, O_2 and temperature on the coral fragment.

For the simulations, the scanned 3D coral geometry was assumed to consist of a tissue layer with an uniform thickness created on top of the skeleton (Figure S1a, S1b), which was placed in a rectangular flow chamber (Figure S1c). Different sub-layers within the coral tissue (Taylor Parkins et al., 2021), with varying material properties and supporting different chemical reactions, were

252 represented indirectly as function of the distance from the tissue-water surface. The model first
253 computes the light field within and around the coral (Figure S1d), then the laminar flow of water
254 around the coral in the flow chamber. Subsequently, mass and heat balances allow calculation of
255 the radiation driven O_2 and temperature distribution in the stratified coral domain and the water
256 column (Figure S1e and S1f). All the model parameters are listed in Table S1 (supplementary
257 information).

258 *Model geometry*

259 The model geometry consisted of a solid domain, the 3D scan of the coral fragment, enclosed by
260 the liquid in a box matching the dimensions of the flow chamber used experimentally (Figure
261 S1c). This geometry was built in COMSOL Multiphysics (v6, COMSOL Inc., Burlington, MA) based
262 on the STL file provided by the coral 3D scanning. Two different orientations of the fragment with
263 respect to the flow (Figure S1) were simulated.

264 An essential part of the model includes the effect of coral tissue sub-layers with various
265 properties, thus assigning different material properties and reactions as a function of depth
266 within the tissue, as done in (Taylor Parkins et al., 2021) albeit in a much simpler geometry.
267 However, an explicit partitioning of the large 3D coral domain in several very thin subdomains on
268 the skeleton surface proved to be very difficult computationally, especially regarding the
269 accurate meshing of these thin layers. We therefore adopted the solution of representing these
270 layers implicitly, by a distance *d* from the coral/water surface. The perpendicular distance (*d*)
271 within the coral from the coral/water surface was computed in COMSOL (the wall-distance
272 interface) by a modified Eikonal equation (Fares & Schröder, 2002). Consequently, the optical,

mass and heat transfer properties characteristic for different tissue sub-layers were defined as a function of this distance, *d*.

Radiative transfer

The scalar irradiance at different positions in the coral and water was determined by calculating the radiative transfer (Figure S1d) using the 3D Monte Carlo (MC) approach implemented in the free software ValoMC (Leino et al., 2019), as described in our previous work (Taylor Parkins et al., 2021). The simulation of photon transport was performed by launching photons with a wavelength of 636 nm, within the Chl *c* and Chl *a* absorption band of the coral microalgal symbionts. The present model ignores fluorescence and takes only scattering and absorption into account. Various tissue layers and skeleton optical properties (OP1, Table S1) were assigned as a function of the calculated wall distance *d*.

The simulated point cloud of scalar irradiance values from ValoMC were imported into COMSOL and mapped over the 3D geometry by solving Poisson's diffusion equation in weak form, in order to smoothen the variations in the scalar irradiance data inherent due to the stochastic nature of the MC simulation:

$$\nabla \cdot \left(f_s h^2 \nabla I_s \right) = I_s - I_0 \qquad (1)$$

where I_s is the smoothed normalised scalar irradiance, I_0 is the initial normalised scalar irradiance, h is the local mesh element size, and f_s is a smoothing factor (0.1; $0 < f_s < 1$). A zero light flux condition was applied to all boundaries.

The simulated scalar irradiance at different positions in the geometry was normalized to the incident scalar irradiance. The results are represented as mean ± standard deviation, averaged over 12 different points, sampled close to each other, as indicated by the squares in Figure 2a.

Fluid flow

Stationary incompressible Navier-Stokes equations for laminar flow (Reynolds number of ~9) were used to simulate the water flow around the coral fragment using COMSOL:

$$\rho(\mathbf{u}\cdot\nabla)\mathbf{u}+\nabla p-\mu\nabla^2\mathbf{u}=0 \quad (2)$$

$$\nabla\cdot\mathbf{u}=0 \quad (3)$$

where **u** is the velocity vector, p the pressure, μ the dynamic viscosity and ρ the density of water. The water inflow had an average velocity of 1 mm s^{-1}, while a zero gauge pressure was set in the outflow. Top, bottom and lateral walls of the flow cell were no-slip (zero-velocity). Two cases were assumed for flow at the coral surface: zero-velocity (without ciliary movement) and a set velocity (with ciliary movement). Ciliary movement as proposed in other studies (Pacherres et al., 2020; Shapiro et al., 2014) was included as cilia-induced currents by assuming an oscillating horizontal velocity component at the coral surface as (Pacherres et al., 2022):

$$u_x = c_{vel}\sin\left(2\frac{\pi}{\delta}x\right) \quad (4)$$

$$u_y = c_{vel}\sin\left(2\frac{\pi}{\delta}y\right) \quad (5)$$

with x and y being the distances from surface, c_{vel} the maximum ciliate beating velocity taken 150 µm s^{-1} as in the previous measurements (Shapiro et al., 2014) and δ the characteristic length scale of the vortices (assumed 1200 µm, close to the average calyx size of the coral).

311 The simulated flow profile around the coral was similar with and without the base onto which
312 the coral was glued (Figure S2). Hence, in order to simplify the geometry and the computational
313 burden, all the simulations presented here were made without the base.

314

315 *Oxygen transport and reactions*

316 The dissolved oxygen concentration, c_{O2}, in the coral and surrounding water was computed from
317 a stationary material balance, written in a general form as eq. (6):

318 $$D_{O2}\nabla^2 c_{O2} - \mathbf{u}\cdot\nabla c_{O2} + R_{O2} + T_{O2} = 0 \qquad (6)$$

319 Diffusive transport was applicable in both domains with diffusion coefficient D_{O2} taking the value
320 $D_{O2,w}$ for dissolved O_2 in water, but reduced values in the coral ($0.5\cdot D_{O2,w}$ in the tissue and
321 $0.01\cdot D_{O2,w}$ in the skeleton). In the water domain there were no reactions involving oxygen (R_{O2}=0),
322 while in the coral tissue/skeleton there was no convective transport (**u**=0). The gas-liquid transfer
323 term T_{O2} accounted for eventual O_2 super-saturation, thus preventing apparition of
324 exaggeratedly high O_2 concentrations in certain areas. A constant O_2 concentration $c_{0,O2}$ was
325 imposed in the water inflow and the classical convection-only condition was assumed in the
326 water outlet, with the rest of flow cell walls insulated (no flux of O_2). The flux and concentration
327 continuity were assumed on the coral/water interface.

328 The net photosynthetic O_2 production rates in oral and aboral gastrodermis (*gas*) were calculated
329 as a function of scalar irradiance I_p using the average light absorption coefficient of the coral
330 tissue $\mu_{a,tis}$:

$$R_{O2,gas} = QE(I_p)\mu_{a,tis} I_p \left(1 - \frac{1}{PR}\right) f_{gas}(d) \quad (7)$$

Here, the quantum efficiency of symbiont photosynthesis (mol O_2 produced per mol photon) is represented as a function $QE(I_p)$ decreasing with increasing scalar irradiance (Figure S3, (Brodersen et al., 2014)). The rate is furthermore limited by the ratio of photosynthesis to respiration rate, *PR*=3.5 (Cooper et al., 2011). f_{gas} is a switch function depending on the distance *d* from the coral/water interface, which allows defining R_{O2} only in the gastrodermis, i.e., f_{gas} = 1 if the distance is 270 – 370 µm for oral, 470 – 570 µm for aboral gastrodermis layer, and f_{gas} = 0 elsewhere.

The respiration rate in the epidermis layer was calculated as function of O_2 concentration c_{O2}:

$$R_{O2,ep} = -R_{ep} \frac{c_{O2}}{K_{O2} + c_{O2}} f_{ep}(d) \quad (8)$$

with R_{ep} the coral host maximum respiration rate and K_{O2} the half-saturation coefficient for O_2 limitation for respiration. Again, the switch function $f_{ep}(d)$ activates this rate (f_{ep} = 1) only at a distance *d* between 90 and 170 µm from the coral surface.

The O_2 consumption in the coral skeleton by endolithic bacteria follows a similar rate:

$$R_{O2,skel} = -R_{cp,skel} \frac{c_{O2}}{K_{O2} + c_{O2}} f_{skel}(d) \quad (9)$$

with $R_{cp,skel}$ the maximum O_2 consumption rate and the same half-saturation coefficient K_{O2}. f_{skel} switches on this rate for *d* > 650 µm and off elsewhere.

Finally, the transfer of dissolved oxygen to gas bubbles at locations with O_2 super saturation in water (at atmospheric saturation) and gastro-vascular cavity domains was included as:

$$T_{O2} = k_l a(c_{s,O2} - c_{O2}) \text{ if } c_{O2} > c_{s,O2}, \quad \text{else } T_{O2} = 0 \tag{10}$$

where $k_l a$ is a gas-liquid exchange coefficient and $c_{s,O2}$ is the O_2 solubility in water.

Heat generation and transport

The spatial temperature *T* distribution in coral and surrounding water was computed from the general heat balance equation including conduction, convection and source terms:

$$k\nabla^2 T - \rho C_p \mathbf{u}\cdot\nabla T + Q = 0 \tag{11}$$

where *k* is the thermal conductivity of the specific layer, C_p and ρ are the specific heat capacity and density of water, *Q* is the heat source and **u** is the vector of water velocity. In particular, heat conduction and generation terms were considered in the coral fragment, while conduction and convection were included in the water domain (neglecting heat generated from light absorption in water). The heat source, *Q*, originates from absorbed light only, which is proportional with the scalar irradiance, I_p, and the light absorption coefficient, μ_a, of the specific layer:

$$Q = f_{heat}\left(I_p\right)\mu_a I_p f_{layer}\left(d\right) \tag{12}$$

where switch functions f_{layer} correspond to specific layers at different distanced from the coral/water surface. $f_{heat}\left(I_p\right)$ is the fraction of light dissipated as heat in the oral and aboral gastrodermis (Figure S4, (Brodersen et al., 2014)), where $f_{heat}<1$ because part of the light energy is used in photosynthesis, while f_{heat} was set to 1 in the other tissue layers and skeleton.

The inflow of water had a temperature of T_0, while a zero-temperature-gradient condition was set for the water outflow. Thermal insulation was set at all other flow-cell walls, while heat flux continuity was assumed at the coral/water interface. The thermal properties of the skeleton were taken from Jimenez et al (Jimenez et al., 2008), while the tissue thermal properties were assigned values similar to human tissue (Hasgall PA, 2018) (due to lack of other measurements).

2.6 Comparison between simulated and measured data

For comparison of measured and simulated scalar irradiance values, scalar irradiance microsensor measurements at 636 nm (normalized to incident irradiance) at the coral tissue/water interface were averaged in different areas of interest over the coral fragment, and were then compared to simulated scalar irradiance values in the same areas of interest (Figure 2). For comparison of measured and simulated O_2 and temperature measurements, we compared measured profiles in particular positions over the coral structure with extracted simulated vertical profiles of O_2 concentration and temperature over the same regions (Figure S5).

3. Results and discussion

We used a combination of microsensor measurements, 3D scanning and numerical modeling to investigate the influence of coral structure and morphology on the light, O_2 and temperature microenvironment in and around a coral fragment (Figure 1). Microsensor measurements are local, making it unfeasibly tedious to map the entire sample and account for spatial heterogeneity

and hot spots. Hence supplementing them with simulations of the light, O_2 concentration and temperature distribution over the 3D morphology of actual samples can help identifying such areas of interest and lead to better data interpretation. On the other hand, supporting simulations with measurements is imperative to realize a physical meaning for the model output, which can also help fine tune certain assumptions, to achieve a more realistic output from the model. Such combination of simulations and microsensor measurements provides a powerful toolset for exploring the coral microenvironment under different flow and light scenarios.

3.1 Light microenvironment

The 3D light simulation generates the distribution of the scalar irradiance within the whole computational domain including water, coral tissue and skeleton. Computed scalar irradiance is displayed at the surface (Figure 2a) and within the coral fragment (Figure 2b). Both the simulations and the light measurements demonstrated the presence of a heterogeneous light field over and within the coral fragment. The computed scalar irradiance shows a fair match with the measurements (Figure 2c) at the same wavelength (636 nm).

Both simulations and the measurements showed that the surface scalar irradiance values (quantified as the ratio of the scalar irradiance over the incident irradiance; mean ± standard deviation, n=12 in each area of interest) were highest at the center of the fragment (measured: 1.40 ± 0.13; simulated: 1.50 ± 0.04; Figure 2a and 2c), where the tissue surface was relatively flat. At the tips of the fragment, the relative scalar irradiance values were lower because the surface was more inclined with respect to the incoming light.

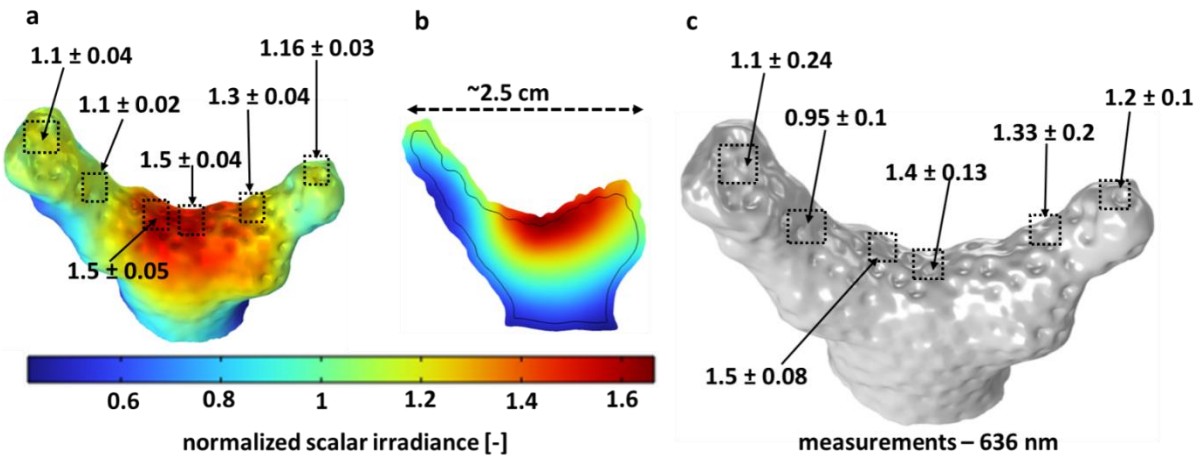

Figure 2: Comparison between measured and simulated scalar irradiance (636 nm; ratio of scalar irradiance to incident irradiance). (a) Simulated scalar irradiance distribution over the coral tissue-water interface; (b) Cross-section of simulated scalar irradiance depth distribution along the middle section of the fragment; (c) Measured scalar irradiance in similar areas, from which simulated values were extracted. Optical properties (OP1) used for simulation are listed in Table S1. The values shown here represent means ± standard deviation, averaged over 12 different points in each area of interest as indicated by the squares.

The rear (shaded) sides of the fragment exhibited much lower scalar irradiance values around half of the incident irradiance (measured and simulated). The simulations indicate that the highest scalar irradiance was close to the tissue-skeleton interface in the middle of the fragment, reaching up to ~1.7 times the incident irradiance (Figure 2b).

Overall, the simulated scalar irradiance at the coral surface compared well to actual measured values in the same regions of the investigated coral. But we note that the light simulations relied on literature values of the inherent optical parameters of coral tissue and skeleton (Jacques et

al., 2019), while the inherent optical properties of coral tissue and skeleton are more complex and involve e.g. different tissue layers with different refractive index (e.g. Wangpraseurt et al., 2014) and tissue regions with more or less scattering and absorption (Wangpraseurt et al., 2019). To illustrate how the model responds to differences in optical parameters, we also simulated the light field in *S. pistillata* fragments using optical parameters determined from OCT measurements (Wangpraseurt et al., 2019) (Figure S6, S7). While the absolute values of scalar irradiance enhancement changed between simulations with different optical parameters, the overall light distribution remained more or less identical between the simulations and reflected the pattern in the experimental light measurements. This highlights the fact that we are still lacking a thorough fine scale characterization of inherent optical properties of coral tissue and skeleton.

The light simulation and measurements revealed an interplay between skeleton and tissue optics that may be important in enhancing coral light harvesting. The light scattering from the skeleton leads to light enhancement in the tissue and a distribution of incident light to shaded areas. For a given direction of the incident light, the distribution of light can vary significantly, even across a small region of a coral colony, leading to hotspots and shaded regions. Light enhancement in a coral fragment is due to a combination of surface morphology and scattering in the tissue and skeleton, which enhances and redistributes light within the fragment (Wangpraseurt et al., 2016). Regions of a coral with relatively flat surfaces (angle of incident light relative to the tissue surface close to 0°) will experience less loss of light due to surface reflections arising from refractive index mismatch, as compared to more inclined surface areas in the colony experiencing lower incident irradiance (due to the cosine dependence of Fresnel reflection on the angle of incidence).

437 However, even shaded regions in a coral colony can receive some light due to lateral distribution
438 of light via the tissue and skeleton (Enríquez et al., 2017; Wangpraseurt et al., 2016;
439 Wangpraseurt et al., 2014).

440 The light field in corals is affected by the optical properties of tissue and skeleton, as well as tissue
441 thickness and composition (e.g. distribution of symbionts and coral host pigments), and overall
442 colony morphology. Hence the irradiance distribution between two morphologically similar coral
443 fragments can vary, and in a reef environment a coral colony could experience varying external
444 and internal light fields throughout the day, depending on the sun angle. Such heterogeneity in
445 the light microenvironment across tissue and over the coral colony surface might present
446 different optical niches that can drive phenotypic or genotypic diversification of symbionts
447 (Lichtenberg et al., 2016) with different light adaptation and bleaching resistance across the same
448 colony or between colonies with different morphology. It is, however, difficult to account for
449 such spatial heterogeneity with microscale light measurements, especially for intra-tissue
450 measurements that often rely on making a small incision in the coral tissue for probe insertion
451 (Wangpraseurt et al., 2012). We show here that simulation of the spatial light distribution in
452 corals with a known morphology and tissue structure is a powerful supplement to fine scale
453 measurements of coral light fields.

454 **3.2 Oxygen microenvironment**

455 The dissolved O_2 distribution in and around a coral colony for a given light field or in darkness is
456 affected by the orientation of the coral with respect to the water flow field. Thus, different parts
457 of the colony will experience changes in the thickness of the MBL and DBL depending on their

458 flow exposure, which will translate into differences in O_2 concentration within and at the surface
459 of tissue.

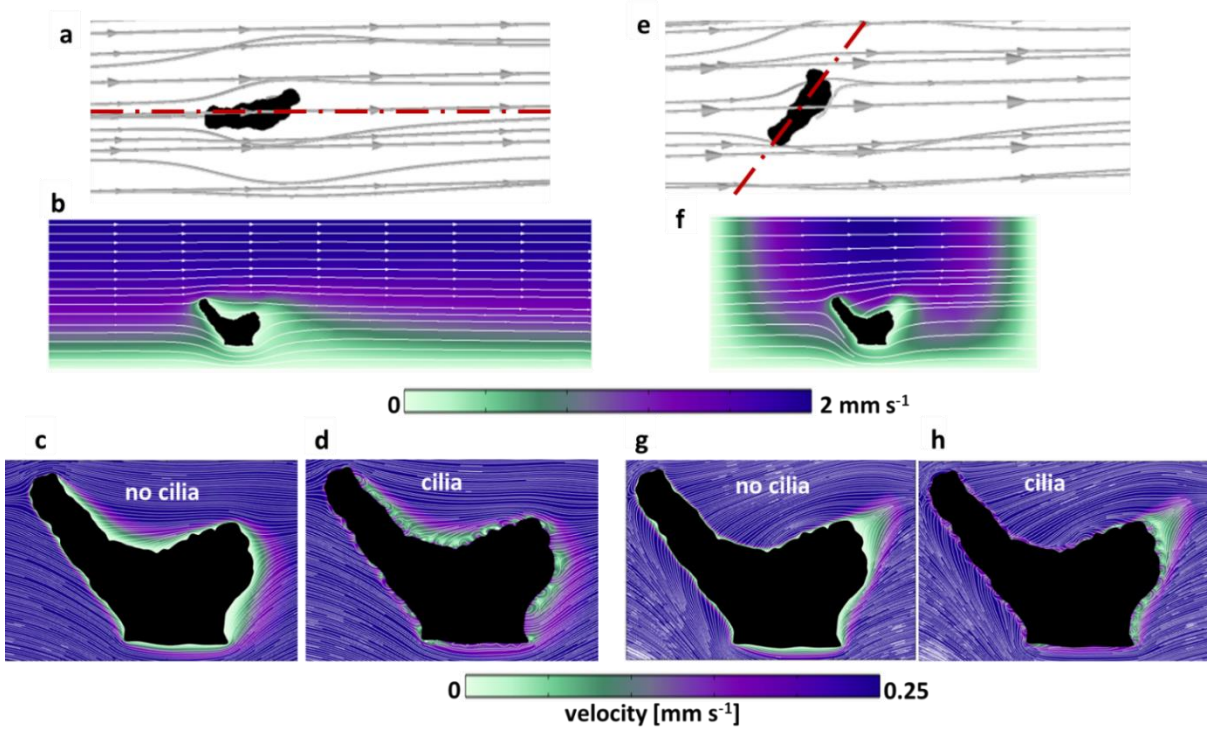

Figure 3: Computed flow field around the coral fragments in two orientations relative to the flow. a,b,c,d: aligned with the flow; e,f,g,h: across the flow. a,e: 3D streamlines of water flowing around the coral fragment. b,f: flow velocity magnitude (color map) and streamlines in the planar sections indicated in (a) and (e) with red dash-dot lines. c,d,g,h: details of velocity magnitude and streamlines in the neighborhood of the coral surface, with and without ciliary movement (same section planes as in b and f, respectively).

460

461

462 The 3D simulations of light-driven O_2 production in the coral fragment within the flow-cell were
463 executed under two fragment orientations with respect to the water flow: with the groove
464 between the two branches shaded against the flow by one branch (Figure 3a), and with the

groove and both branches directly exposed to the flow (Figure 3e). The simulations showed higher O_2 concentration in parts of the fragment that were shaded from the flow and exhibited a thicker DBL, as compared to more exposed areas (Figure 4a, d). The O_2 concentration was high at the skeleton/tissue interface, due to the low diffusivity of the skeleton matrix (Figure 4b, c, e, and f).

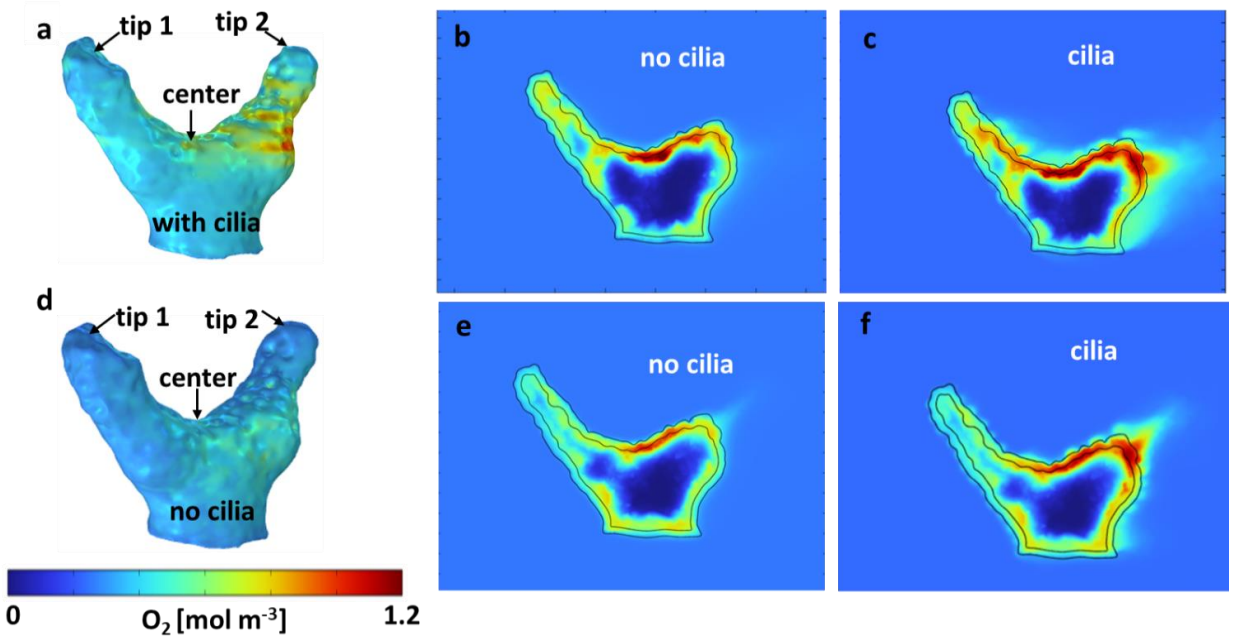

Figure 4: Computed dissolved O_2 concentration in and around the coral fragment. a,b,c: coral fragment aligned with the flow; d,e,f: coral fragment across the flow. a,d: 3D O_2 distribution on the coral (tissue/water) surface. b,e: 2D cross-sections of O_2 concentration without ciliary movement. c,f: 2D cross-sections of oxygen concentration with ciliary movement. The flow direction and 2D sectioning planes are indicated in Figure 3a and 3e.

When the coral fragment was oriented with one branch facing the flow (named aligned with the flow in Figure 3a), the groove and the second branch exhibited a thicker DBL (Figure 3b), as compared to the orientation across the flow (Figure 3e, 3f) where the groove of the fragment

was more flow-exposed. By constructing iso-velocity lines (IVL) at, for example, 1 mm s^{-1}, the hydrodynamic boundary layer, in the more closed-groove orientation appears thicker (Figure S8a). This indicates a retarded water flow, as compared to a more open-groove orientation (Figure S8b) that showed IVL more conformal and closer to the coral surface. Vertical O_2 concentration profiles extracted from the simulated O_2 distributions (Figure S5) were compared with O_2 microsensor measurements done within similar areas of the fragment, and showed a fairly good match (Figure 5) for the two different orientations of the fragment with respect to the water flow.

Under low or no flow conditions, mass transfer and therefore O_2 concentration in corals can also be affected by the movement of cilia covering the coral ectoderm, which can create vortices and some advective transport at the coral tissue surface (Pacherres et al., 2020; Pacherres, 2022). We investigated the role of the ciliated coral tissue surface by comparing O_2 microenvironment simulations with and without ciliary beating (Figure 4b, c). When no cilia beating was included, the simulations indicate a pronounced O_2 accumulation at the center of the fragment (Figure 4b).

Whereas, when cilia movement was included, the simulated O_2 distribution was more homogenous due to enhanced advective transport by the ciliary vortex formation (Figure 4c), in line with published experimental data (Pacherres et al., 2020). The comparison between simulated O_2 profiles and the corresponding measurements (Figure 5a-c) also showed a closer match when cilia beating was included in the model. However, when the coral fragment was oriented across the flow, the central area was more exposed and the MBL was relatively thin.

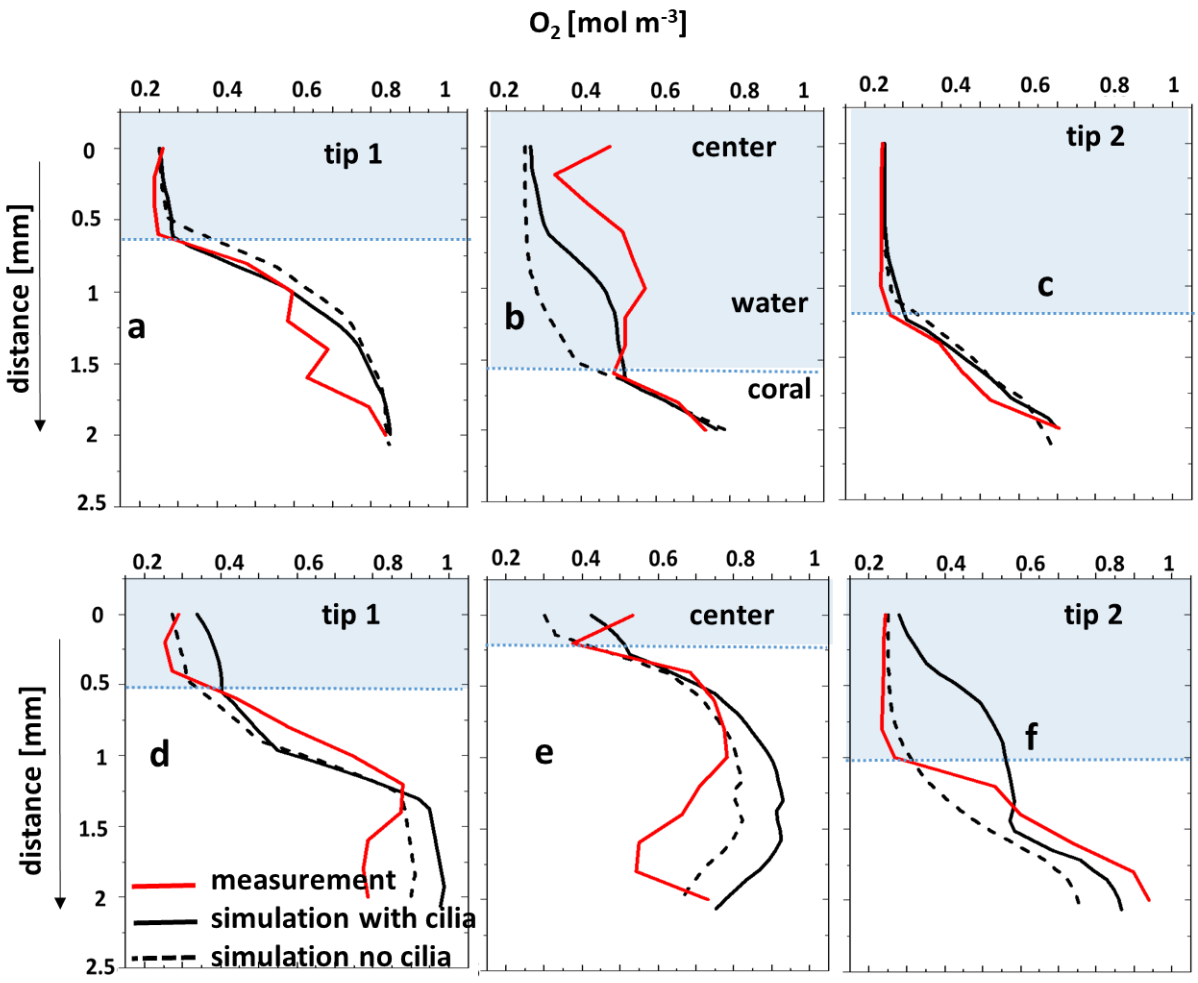

Figure 5: Comparison between microsensor-measured O_2 profiles and the corresponding simulated profiles through the water column and tissue, with and without considering the surface ciliary motion. Coral fragment, a,b,c: aligned with the flow; d,e,f: across the flow. "center", "tip 1" and "tip 2" measurement positions are indicated in Figure 4. The tissue/water boundary indicated here was determined from the simulated DO profile and compared with the measurements.

493

Consequently, the measured and simulated O_2 concentration profiles indicated a smaller impact of the ciliary movements on mass transfer (Figure 4d-f, 5d-f). This suggests that cilia-induced advective transport has a more significant effect on the O_2 transport between the coral tissue and the surrounding seawater in colony regions with slow flow. We note that movements in the coral such as tissue-contraction and expansion and tentacle movement, which are presently not included in the model, could also potentially influence the O_2 mass transport (Malul et al., 2020; Patterson, 1992).

3.3 Temperature microenvironment

Heat transfer simulations and temperature measurements were executed for both orientations of the coral sample with respect to the flow (Figure 6 - aligned; Figure S9 - across). The simulated temperature profiles with and without ciliary movement were very similar, showing an increase of less than 0.2°C, as visible in the 2D cross-sectional images of the computed temperature distribution (Figure 6b,c and Figure S9b,c) and extracted profiles (Figure 6d-f and Figure S9d-f). Temperature profiles measured at three different locations (Figure 6a, S9a) in the fragment were within the range of simulated temperatures, but with considerable noise. The water flow affected local heat transfer, where the temperature simulations show higher tissue heating from the absorbed light in fragment regions exposed to slower flow, albeit the absolute temperature increase was very moderate for the investigated branched coral.

Simulations indicate that the slower heat transfer (thicker MBL and TBL) over tissue regions less exposed to flow was not significantly enhanced by ciliary movement. The temperature increase

514 was highest near the skeleton/tissue interface, due to heat-insulating properties of the skeleton

515 (Jimenez et al., 2008).

516

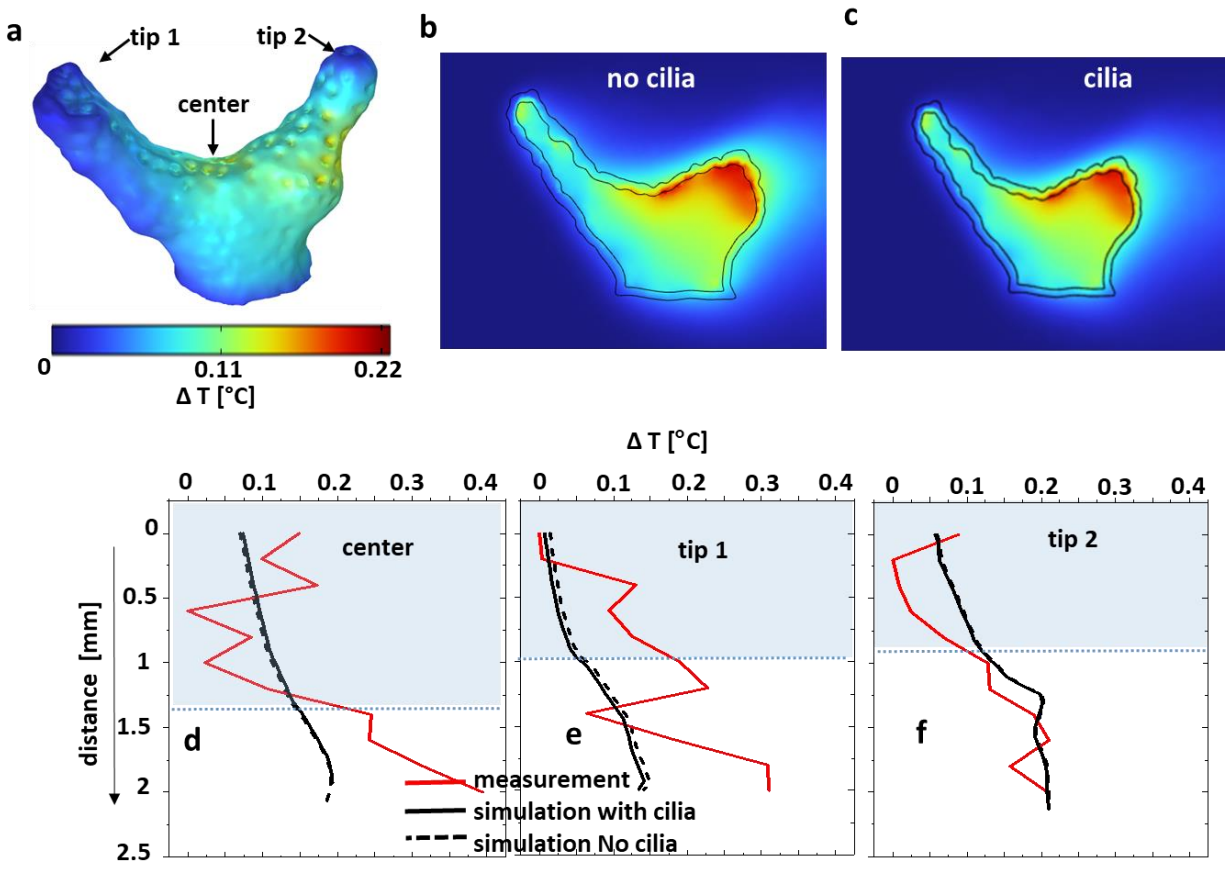

Figure 6: Comparison between measured and simulated temperature distribution for the coral fragment aligned with the flow. The temperature differences ΔT are between the local values and the inflow temperature. a: computed 3D ΔT on the coral (tissue/water) surface; b,c: ΔT in 2D cross-sections through the coral without and with ciliary movement. Sectioning planes are indicated in Figure 3a. d,e,f: measured and simulated temperature difference profiles through the water column and tissue, with and without considering the surface ciliary motion.

Clearly, it is difficult to make a systematic comparison between simulated and measured temperature profiles in this case (Figure 6d-f and Figure S9d-f) due to the very small temperature gradient between coral tissue and water close to the noise level of the microsensor measurements. The small temperature differences in the branched coral fragment are due to a high surface area to volume ratio (Jimenez et al., 2008), allowing a quick heat dissipation into the environment. There is thus a need for more accurate temperature microsensors, but it could also be relevant to compare simulated and measured temperatures on massive corals that have been shown to exhibit a stronger heating than branched corals (Jimenez et al., 2008; Jimenez et al., 2011; Jimenez et al., 2012). Last but not least, there is a lack of thermal property measurements in the different layers in coral tissue, and our simulation of the temperature microenvironment thus largely relied on values for tissue thermal properties from the biomedical literature.

3.4 Outlook

We developed a multiphysics modelling approach that enables simulation of the physico-chemical microenvironment of corals with a known 3D structure under defined irradiance and laminar flow conditions similar to commonly used flow chamber experimental setups. The model results were evaluated on 3D scanned coral samples, previously characterized with microsensor measurements of light, temperature and O_2 in a laminar flow chamber. Such comparison generally showed a good agreement between measured and simulated data, but several model improvements can be considered for future work. The current model only considers light of individual wavelengths at a time and does not include inelastic scattering (e.g. conversion of light energy due to fluorescence). Broadband spectral simulations would e.g. enable simulations of how the spectral red shifts caused by fluorescent host pigments (Alieva et al., 2008; Salih et al.,

2000), wavelength-specific reflectivity by chromoproteins (Alieva et al., 2008; D'Angelo et al., 2008) affect the coral light field and photosynthesis (Ben-Zvi et al., 2021), internal heat generation (Quick et al., 2018), as well as coral bleaching and recovery (Grinblat et al., 2018). However, an important prerequisite for more detailed simulations would be a better quantification of the inherent optical and thermal properties of coral tissue and skeleton, which are still very scarce in the literature. The present models therefore partially rely on assumed thermal property values taken from biomedical tissue studies.

The simple laminar flow scenario currently implemented in the present study does not cover all flow scenarios of corals *in situ* , and is more representative of calm sea conditions on reef flats and inside coral patches (Jimenez et al., 2011; Jimenez et al., 2012), as well as in many experimental flow chambers used for ecophysiological studies of coral metabolism. It is possible to include more complex flow scenarios in our modeling approach such as turbulent and oscillating flows (Ong et al., 2012; Ong et al., 2012), albeit at higher computational costs. Furthermore, it would be interesting to compare simulated and measured flow fields around corals, e.g. using particle imaging velocimetry (Pacherres et al., 2020) or combined measurements of flow and O_2 fields around corals (Ahmerkamp et al., 2022; Pacherres et al., 2022). The latter could also enable implementation of a more detailed account for the role of ciliary movement for coral mass and heat transfer.

The present model only accounts for photosynthetic O_2 production of symbionts using a simple approach based on reported quantum efficiencies, while O_2 consumption by respiration in different tissue layers is partially based on published values and P/R relationships. The model could be expanded to better account for photosynthetic light saturation and photoinhibition.

Considering other chemical species (inorganic and organic carbon, various acid/base couples) and reactions in our model would enable the representation of calcification and carbon transfer between symbionts and host, and such work is in progress. Another desired expansion could be a more detailed account of metabolic processes in the coral skeleton, performed by the endolithic algae and microbes (Ricci et al., 2019; Tandon et al., 2022).

Furthermore, the present model assumes homogenous tissue thickness over the coral colony and does not include an accurate representation of fine scale topographic and anatomic features of coral tissue and skeleton, such as the polyps with tentacles and a complex internal gastrovascular system, and the more homogenous connective tissue between polyps. Our model also represents coral tissue as a static structure. This is a simplification, as corals exhibit pronounced tissue plasticity via contraction and expansion, which can strongly affect surface area to volume ratios (Patterson, 1992) and optical properties (Wangpraseurt et al., 2017), which in turn modulate mass, heat and radiative transfer processes. More precise tomographic mapping of coral tissue and skeleton morphology and thickness e.g. with µCT scanning or OCT, in combination with including fluid-structure interaction models with moving interfaces (Taherzadeh et al., 2012) could allow for simulating effects of coral topography and mechanics on the coral microenvironment, but this will require substantial computational resources.

Finally, the presented 3D modelling approach can also be used to simulate different time-dependent environmental conditions (e.g., variable flow, day-night hypoxia, different solar irradiation regimes), which can help evaluating mechanisms driving coral stress responses as well as basic niche shaping factors for symbionts and microbiomes in the coral holobiont. The model

582 could also be useful in more applied research such as in the ongoing attempts to create bionic
583 corals (Wangpraseurt et al., 2022; Wangpraseurt et al., 2020) or for optimization of other 3D
584 bioprinted constructs (Krujatz et al., 2022), where different designs can be evaluated and
585 optimized. Our approach is also relevant for simulating structure-function relationships in other
586 benthic systems such as photosynthetic biofilms and aquatic plant tissue, and can also be
587 adapted to other sessile organisms such as symbiont-bearing giant clams, ascidians, jellyfish or
588 foraminifera.

589 # 4. Conclusion

590 We developed a 3D multiphysics model to simulate the spatial distribution of light, O_2 and
591 temperature (and the corresponding radiative, mass and heat transfer) across a stratified coral
592 tissue, skeleton and around natural coral morphologies exposed to a defined flow field and
593 incident irradiance. Model results compared well with spatial measurements of light, O_2 and
594 temperature under similar flow and light conditions. The model reveals how the interaction
595 between incident irradiance, water flow and complex coral morphology leads to pronounced
596 spatial heterogeneity and microenvironments, both across tissue layers and between different
597 areas of the coral. Such simulation of the physico-chemical microenvironmental landscape using
598 real 3D scanned coral structures as an input, can i) give insights to coral tissue and skeleton
599 compartments that are difficult to reach with existing sensor technology, and ii) identify hotspots
600 of activity that can inform detailed measurements e.g. with microsensors and/or various
601 bioimaging techniques for mapping structure and function. The model can simulate effects of
602 different environmental (e.g. light, temperature, hypoxia or flow) and structural (e.g. symbiont

603 and host pigment density and distribution, and the distribution of endolithic microbes) factors
604 on the coral microenvironment and metabolic activity, which can be tested experimentally. We
605 argue that such combination of modeling and experimental investigation is a strong tool set for
606 unravelling structure-function relations and basic regulatory mechanisms in coral biology and
607 stress responses, including effects of climate change and other anthropogenic threats.

608 Acknowledgements

609 We acknowledge technical assistance with coral husbandry by Sofie Jakobsen, Victoria Thuesen
610 and Caroline Vigsbo Christensen. This study was funded by the Gordon and Betty Moore
611 Foundation through grant no. GBMF9206 to M.K. (https://doi.org/10.37807/GBMF9206). C.P.
612 acknowledges support and access to computational resources offered by the KAUST Computing
613 Center.

614 Competing interests

615 The authors declare no competing interest.

616 Author Contributions

617 S.M., C.P. and M.K. designed the research. S.M. developed the coral model, performed computer
618 simulations and measurements. S.M., C.P. and M.K. analyzed the data. S.M., C.P. and M.K. wrote
619 the manuscript. C.P. and M.K. provided research infrastructure.

620 Data availability

621 All data will be made available in Dyrad, and scripts of the modeling approaches are available
622 from the authors at reasonable request.

References

Ahmerkamp, S., Jalaluddin, F. M., Cui, Y., Brumley, D. R., Pacherres, C. O., Berg, J. S., Stocker, R., Kuypers, M. M. M., Koren, K., & Behrendt, L. (2022). Simultaneous visualization of flow fields and oxygen concentrations to unravel transport and metabolic processes in biological systems. *Cell Reports Methods*, *2*(5), 100216. https://doi.org/https://doi.org/10.1016/j.crmeth.2022.100216

Al-Horani, F. A., Al-Moghrabi, S. M., & de Beer, D. (2003). The mechanism of calcification and its relation to photosynthesis and respiration in the scleractinian coral Galaxea fascicularis. *Marine Biology*, *142*(3), 419-426. https://doi.org/10.1007/s00227-002-0981-8

Alieva, N. O., Konzen, K. A., Field, S. F., Meleshkevitch, E. A., Hunt, M. E., Beltran-Ramirez, V., Miller, D. J., Wiedenmann, J., Salih, A., & Matz, M. V. (2008). Diversity and evolution of coral fluorescent proteins. *PLoS ONE*, *3*(7), e2680. https://doi.org/10.1371/journal.pone.0002680

Altieri, A. H., Harrison, S. B., Seemann, J., Collin, R., Diaz, R. J., & Knowlton, N. (2017). Tropical dead zones and mass mortalities on coral reefs. *Proceedings of the National Academy of Sciences*, *114*(14), 3660-3665. https://doi.org/doi:10.1073/pnas.1621517114

Anthony, K. R. N., & Hoegh-Guldberg, O. (2003). Variation in Coral Photosynthesis, Respiration and Growth Characteristics in Contrasting Light Microhabitats: An Analogue to Plants in Forest Gaps and Understoreys? *Functional Ecology*, *17*(2), 246-259. http://www.jstor.org/stable/3599181

Ben-Zvi, O., Wangpraseurt, D., Bronstein, O., Eyal, G., & Loya, Y. (2021). Photosynthesis and Bio-Optical Properties of Fluorescent Mesophotic Corals [Original Research]. *Frontiers in Marine Science*, *8*. https://doi.org/10.3389/fmars.2021.651601

Bollati, E., Lyndby, N. H., D'Angelo, C., Kühl, M., Wiedenmann, J., & Wangpraseurt, D. (2022). Green fluorescent protein-like pigments optimise the internal light environment in symbiotic reef-building corals. *Elife*, *11*, e73521. https://doi.org/10.7554/eLife.73521

Brodersen, K. E., Lichtenberg, M., Ralph, P. J., Kühl, M., & Wangpraseurt, D. (2014). Radiative energy budget reveals high photosynthetic efficiency in symbiont-bearing corals. *Journal of The Royal Society Interface*, *11*(93), 20130997. https://doi.org/doi:10.1098/rsif.2013.0997

Chalker, B. E. (1981). Simulating light-saturation curves for photosynthesis and calcification by reef-building corals. *Marine Biology*, *63*(2), 135-141. https://doi.org/10.1007/BF00406821

Chan, N. C. S., Wangpraseurt, D., Kühl, M., & Connolly, S. R. (2016). Flow and Coral Morphology Control Coral Surface pH: Implications for the Effects of Ocean Acidification [Original Research]. *Frontiers in Marine Science*, *3*. https://doi.org/10.3389/fmars.2016.00010

Chang, S., Iaccarino, G., Ham, F., Elkins, C., & Monismith, S. (2014). Local shear and mass transfer on individual coral colonies: Computations in unidirectional and wave-driven flows. *Journal of Geophysical Research: Oceans*, *119*(4), 2599-2619. https://doi.org/https://doi.org/10.1002/2013JC009751

Chindapol, N., Kaandorp, J. A., Cronemberger, C., Mass, T., & Genin, A. (2013). Modelling growth and form of the scleractinian coral Pocillopora verrucosa and the influence of hydrodynamics. *PLoS Comput Biol*, *9*(1), e1002849. https://doi.org/10.1371/journal.pcbi.1002849

Cooper, T. F., Ulstrup, K. E., Dandan, S. S., Heyward, A. J., Kühl, M., Muirhead, A., O'Leary, R. A., Ziersen, B. E. F., & Van Oppen, M. J. H. (2011). Niche specialization of reef-building corals in the mesophotic zone: metabolic trade-offs between divergent Symbiodinium types. *Proceedings of the Royal Society B: Biological Sciences*, *278*(1713), 1840-1850. https://doi.org/doi:10.1098/rspb.2010.2321

Costanza, R., de Groot, R., Sutton, P., van der Ploeg, S., Anderson, S. J., Kubiszewski, I., Farber, S., & Turner, R. K. (2014). Changes in the global value of ecosystem services. *Global Environmental Change*, *26*, 152-158. https://doi.org/https://doi.org/10.1016/j.gloenvcha.2014.04.002

669 D'Angelo, C., Denzel, A., Vogt, A., Matz, M., Oswald, F., Salih, A., Nienhaus, G., & Wiedenmann, J. (2008).
670 Blue light regulation of host pigment in reef-building corals. *Marine Ecology-progress Series -*
671 *MAR ECOL-PROGR SER*, *364*, 97-106. https://doi.org/10.3354/meps07588
672 Davy, S. K., Allemand, D., & Weis, V. M. (2012). Cell Biology of Cnidarian-Dinoflagellate Symbiosis.
673 *Microbiology and Molecular Biology Reviews*, *76*(2), 229-261.
674 https://doi.org/doi:10.1128/MMBR.05014-11
675 Dubinsky, Z., Falkowski, P. G., Porter, J. W., Muscatine, L., & Smith, D. C. (1984). Absorption and
676 utilization of radiant energy by light- and shade-adapted colonies of the hermatypic coral
677 Stylophora pistillata. *Proceedings of the Royal Society of London. Series B. Biological Sciences*,
678 *222*(1227), 203-214. https://doi.org/doi:10.1098/rspb.1984.0059
679 Dunne, R. P., & Brown, B. E. (2001). The influence of solar radiation on bleaching of shallow water reef
680 corals in the Andaman Sea, 1993-1998 [Article]. *Coral Reefs*, *20*(3), 201-210.
681 https://doi.org/10.1007/s003380100160
682 Enríquez, S., Méndez, E. R., & -Prieto, R. I. (2005). Multiple scattering on coral skeletons enhances light
683 absorption by symbiotic algae. *Limnology and Oceanography*, *50*(4), 1025-1032.
684 https://doi.org/https://doi.org/10.4319/lo.2005.50.4.1025
685 Enríquez, S., Méndez, E. R., Hoegh-Guldberg, O., & Iglesias-Prieto, R. (2017). Key functional role of the
686 optical properties of coral skeletons in coral ecology and evolution. *Proc Biol Sci*, *284*(1853).
687 https://doi.org/10.1098/rspb.2016.1667
688 Eyal, G., Wiedenmann, J., Grinblat, M., D'Angelo, C., Kramarsky-Winter, E., Treibitz, T., Ben-Zvi, O.,
689 Shaked, Y., Smith, T. B., Harii, S., Denis, V., Noyes, T., Tamir, R., & Loya, Y. (2015). Spectral
690 Diversity and Regulation of Coral Fluorescence in a Mesophotic Reef Habitat in the Red Sea.
691 *PLoS ONE*, *10*(6), e0128697. https://doi.org/10.1371/journal.pone.0128697
692 Fares, E., & Schröder, W. (2002). A differential equation for approximate wall distance. *International*
693 *Journal for Numerical Methods in Fluids*, *39*(8), 743-762.
694 https://doi.org/https://doi.org/10.1002/fld.348
695 Goreau, T. J., Goreau, N. I., Trench, R. K., & Hayes, R. L. (1996). Calcification Rates in Corals. *Science*,
696 *274*(5284), 117-117. https://doi.org/doi:10.1126/science.274.5284.117-b
697 Grinblat, M., Fine, M., Tikochinski, Y., & Loya, Y. (2018). Stylophora pistillata in the Red Sea demonstrate
698 higher GFP fluorescence under ocean acidification conditions. *Coral Reefs*, *37*(1), 309-320.
699 https://doi.org/10.1007/s00338-018-1659-0
700 Hasgall PA, D. G. F., Baumgartner C, Neufeld E, Lloyd B, Gosselin MC, Payne D, Klingenböck A, Kuster N (
701 2018). *IT'IS Database for thermal and electromagnetic parameters of biological tissues*.
702 https://doi.org/ DOI: 10.13099/VIP21000-04-0. itis.swiss/database
703 Hughes, D. J., Alderdice, R., Cooney, C., Kühl, M., Pernice, M., Voolstra, C. R., & Suggett, D. J. (2020).
704 Coral reef survival under accelerating ocean deoxygenation. *Nature Climate Change*, *10*(4), 296-
705 307. https://doi.org/10.1038/s41558-020-0737-9
706 Hughes, D. J., Raina, J.-B., Nielsen, D. A., Suggett, D. J., & Kühl, M. (2022). Disentangling compartment
707 functions in sessile marine invertebrates. *Trends in Ecology & Evolution*, *37*(9), 740-748.
708 https://doi.org/https://doi.org/10.1016/j.tree.2022.04.008
709 Hughes, T. P., Kerry, J. T., Álvarez-Noriega, M., Álvarez-Romero, J. G., Anderson, K. D., Baird, A. H.,
710 Babcock, R. C., Beger, M., Bellwood, D. R., Berkelmans, R., Bridge, T. C., Butler, I. R., Byrne, M.,
711 Cantin, N. E., Comeau, S., Connolly, S. R., Cumming, G. S., Dalton, S. J., Diaz-Pulido, G., Eakin, C.
712 M., Figueira, W. F., Gilmour, J. P., Harrison, H. B., Heron, S. F., Hoey, A. S., Hobbs, J.-P. A.,
713 Hoogenboom, M. O., Kennedy, E. V., Kuo, C.-y., Lough, J. M., Lowe, R. J., Liu, G., McCulloch, M.
714 T., Malcolm, H. A., McWilliam, M. J., Pandolfi, J. M., Pears, R. J., Pratchett, M. S., Schoepf, V.,
715 Simpson, T., Skirving, W. J., Sommer, B., Torda, G., Wachenfeld, D. R., Willis, B. L., & Wilson, S. K.

(2017). Global warming and recurrent mass bleaching of corals. *Nature*, *543*(7645), 373-377. https://doi.org/10.1038/nature21707

Jackson, J. B. C., Kirby, M. X., Berger, W. H., Bjorndal, K. A., Botsford, L. W., Bourque, B. J., Bradbury, R. H., Cooke, R., Erlandson, J., Estes, J. A., Hughes, T. P., Kidwell, S., Lange, C. B., Lenihan, H. S., Pandolfi, J. M., Peterson, C. H., Steneck, R. S., Tegner, M. J., & Warner, R. R. (2001). Historical Overfishing and the Recent Collapse of Coastal Ecosystems. *Science*, *293*(5530), 629-637. https://doi.org/doi:10.1126/science.1059199

Jacques, S. L., Wangpraseurt, D., & Kühl, M. (2019). Optical Properties of Living Corals Determined With Diffuse Reflectance Spectroscopy [Original Research]. *Frontiers in Marine Science*, *6*(472). https://doi.org/10.3389/fmars.2019.00472

Jimenez, I. M., Kühl, M., Larkum, A. W. D., & Ralph, P. J. (2008). Heat budget and thermal microenvironment of shallow-water corals: Do massive corals get warmer than branching corals? *Limnology and Oceanography*, *53*(4), 1548-1561. https://doi.org/https://doi.org/10.4319/lo.2008.53.4.1548

Jimenez, I. M., Kühl, M., Larkum, A. W. D., & Ralph, P. J. (2011). Effects of flow and colony morphology on the thermal boundary layer of corals. *Journal of The Royal Society Interface*, *8*(65), 1785-1795. https://doi.org/doi:10.1098/rsif.2011.0144

Jimenez, I. M., Larkum, A. W. D., Ralph, P. J., & Kühl, M. (2012). In situ thermal dynamics of shallow water corals is affected by tidal patterns and irradiance. *Marine Biology*, *159*(8), 1773-1782. https://doi.org/10.1007/s00227-012-1968-8

Johnson, M. D., Rodriguez, L. M., & Altieri, A. H. (2018). Shallow-water hypoxia and mass mortality on a Caribbean coral reef. *Bulletin of Marine Science*, *94*(1), 143-144. https://doi.org/10.5343/bms.2017.1163.

Kaniewska, P., Magnusson, S. H., Anthony, K. R., Reef, R., Kühl, M., & Hoegh-Guldberg, O. (2011). IMPORTANCE OF MACRO- VERSUS MICROSTRUCTURE IN MODULATING LIGHT LEVELS INSIDE CORAL COLONIES(1). *J Phycol*, *47*(4), 846-860. https://doi.org/10.1111/j.1529-8817.2011.01021.x

Kaniewska, P., & Sampayo, E. M. (2022). Macro- and micro-scale adaptations allow distinct Stylophora pistillata-symbiodiniaceae holobionts to optimize performance across a broad light habitat. *J Phycol*, *58*(1), 55-70. https://doi.org/10.1111/jpy.13215

Knowlton, N., Corcoran, E., Felis, T., de Goeij, J., Grottoli, A., Harding, S., Kleypas, J., Mayfield, A., Miller, M., & Obura, D. (2021). Rebuilding coral reefs: a decadal grand challenge. https://doi.org/10.53642/NRKY9386

Kramer, N., Guan, J., Chen, S., Wangpraseurt, D., & Loya, Y. (2022). Morpho-functional traits of the coral Stylophora pistillata enhance light capture for photosynthesis at mesophotic depths. *Communications Biology*, *5*(1), 861. https://doi.org/10.1038/s42003-022-03829-4

Krujatz, F., Dani, S., Windisch, J., Emmermacher, J., Hahn, F., Mosshammer, M., Murthy, S., Steingröwer, J., Walther, T., Kühl, M., Gelinsky, M., & Lode, A. (2022). Think outside the box: 3D bioprinting concepts for biotechnological applications - recent developments and future perspectives. *Biotechnology advances*, *58*, 107930. https://doi.org/10.1016/j.biotechadv.2022.107930

Kühl, M., Holst, G., Larkum, A. W., & Ralph, P. J. (2008). IMAGING OF OXYGEN DYNAMICS WITHIN THE ENDOLITHIC ALGAL COMMUNITY OF THE MASSIVE CORAL PORITES LOBATA(1). *J Phycol*, *44*(3), 541-550. https://doi.org/10.1111/j.1529-8817.2008.00506.x

Kaandorp, J. A. (2013). Macroscopic Modelling of Environmental Influence on Growth and Form of Sponges and Corals Using the Accretive Growth Model. *International Scholarly Research Notices*, *2013*, 1-14. https://doi.org/10.1155/2013/159170

LaJeunesse, T. C., Parkinson, J. E., Gabrielson, P. W., Jeong, H. J., Reimer, J. D., Voolstra, C. R., & Santos, S. R. (2018). Systematic Revision of Symbiodiniaceae Highlights the Antiquity and Diversity of

764 Coral Endosymbionts. *Current Biology*, *28*(16), 2570-2580.e2576.
765 https://doi.org/https://doi.org/10.1016/j.cub.2018.07.008
766 Leino, A. A., Pulkkinen, A., & Tarvainen, T. (2019). ValoMC: a Monte Carlo software and MATLAB toolbox
767 for simulating light transport in biological tissue. *Osa Continuum*, *2*(3), 957-972.
768 https://doi.org/10.1364/Osac.2.000957
769 Lichtenberg, M., Larkum, A. W. D., & Kühl, M. (2016). Photosynthetic Acclimation of Symbiodinium in
770 hospite Depends on Vertical Position in the Tissue of the Scleractinian Coral Montastrea curta
771 [Original Research]. *Frontiers in Microbiology*, *7*. https://doi.org/10.3389/fmicb.2016.00230
772 Loya, Y., Sakai, K., Yamazato, K., Nakano, Y., Sambali, H., & Van Woesik, R. (2001). Coral bleaching: The
773 winners and the losers [Article]. *Ecology Letters*, *4*(2), 122-131. https://doi.org/10.1046/j.1461-
774 0248.2001.00203.x
775 Lyndby, N. H., Kühl, M., & Wangpraseurt, D. (2016). Heat generation and light scattering of green
776 fluorescent protein-like pigments in coral tissue. *Scientific Reports*, *6*(1), 26599.
777 https://doi.org/10.1038/srep26599
778 Malul, D., Holzman, R., & Shavit, U. (2020). Coral tentacle elasticity promotes an out-of-phase
779 motion that improves mass transfer. *Proceedings of the Royal Society B: Biological Sciences*,
780 *287*(1929), 20200180. https://doi.org/doi:10.1098/rspb.2020.0180
781 Moberg, F., & Folke, C. (1999). Ecological goods and services of coral reef ecosystems. *Ecological*
782 *Economics*, *29*(2), 215-233. https://doi.org/https://doi.org/10.1016/S0921-8009(99)00009-9
783 Mumby, P. J., Chisholm, J. R. M., Edwards, A. J., Andrefouet, S., & Jaubert, J. (2001). Cloudy weather may
784 have saved Society Island reef corals during the 1998 ENSO event [Article]. *Marine Ecology*
785 *Progress Series*, *222*, 209-216. https://doi.org/10.3354/meps222209
786 Muscatine, L. (1973). 4. - NUTRITION OF CORALS. In O. A. Jones & R. Endean (Eds.), *Biology and Geology*
787 *of Coral Reefs* (pp. 77-115). Academic Press. https://doi.org/https://doi.org/10.1016/B978-0-12-
788 395526-5.50012-2
789 Nakamura, T., Yamasaki, H., & Van Woesik, R. (2003). Water flow facilitates recovery from bleaching in
790 the coral Stylophora pistillata [Article]. *Marine Ecology Progress Series*, *256*, 287-291.
791 https://doi.org/10.3354/meps256287
792 Ong, R. H., King, A. J., Mullins, B. J., Cooper, T. F., & Caley, M. J. (2012). Development and validation of
793 computational fluid dynamics models for prediction of heat transfer and thermal
794 microenvironments of corals. *PLoS ONE*, *7*(6), e37842.
795 https://doi.org/10.1371/journal.pone.0037842
796 Ong, R. H., King, A. J. C., Caley, M. J., & Mullins, B. J. (2018). Prediction of solar irradiance using ray-
797 tracing techniques for coral macro- and micro-habitats. *Marine Environmental Research*, *141*,
798 75-87. https://doi.org/https://doi.org/10.1016/j.marenvres.2018.08.004
799 Ong, R. H., King, A. J. C., Kaandorp, J. A., Mullins, B. J., & Caley, M. J. (2017). The effect of allometric
800 scaling in coral thermal microenvironments. *PLoS ONE*, *12*(10), e0184214.
801 https://doi.org/10.1371/journal.pone.0184214
802 Ong, R. H., King, A. J. C., Mullins, B. J., & Caley, M. J. (2019). The effect of small-scale morphology on
803 thermal dynamics in coral microenvironments. *Journal of Thermal Biology*, *86*, 102433.
804 https://doi.org/https://doi.org/10.1016/j.jtherbio.2019.102433
805 Ong, R. H., King, A. J. C., Mullins, B. J., Caley, M. J., & Cooper, T. F. (2012). CFD Simulation of Low
806 Reynolds-number Turbulence Models in Coral Thermal Microenvironment.
807 http://hdl.handle.net/20.500.11937/13242
808 Pacherres, C. O., Ahmerkamp, S., Schmidt-Grieb, G. M., Holtappels, M., & Richter, C. (2020). Ciliary
809 vortex flows and oxygen dynamics in the coral boundary layer. *Scientific Reports*, *10*(1), 7541.
810 https://doi.org/10.1038/s41598-020-64420-7

Pacherres, C. O. a. A., Soeren and Koren, Klaus and Richter, Claudio and Holtappels, Moritz. (2022). Ciliary Flows in Corals Ventilate Target Areas of High Photosynthetic Oxygen Production. https://doi.org/10.1016/j.cub.2022.07.071

Patterson, M. R. (1992). A Chemical Engineering View of Cnidarian Symbioses. *American Zoologist*, *32*(4), 566-582. http://www.jstor.org/stable/3883702

Quick, C., D'Angelo, C., & Wiedenmann, J. (2018). Trade-Offs Associated with Photoprotective Green Fluorescent Protein Expression as Potential Drivers of Balancing Selection for Color Polymorphism in Reef Corals. *Frontiers in Marine Science*, *5*. https://doi.org/10.3389/fmars.2018.00011

Revsbech, N. P. (1989). An oxygen microsensor with a guard cathode. *Limnology and Oceanography*, *34*(2), 474-478. https://doi.org/https://doi.org/10.4319/lo.1989.34.2.0474

Ricci, F., Rossetto Marcelino, V., Blackall, L. L., Kühl, M., Medina, M., & Verbruggen, H. (2019). Beneath the surface: community assembly and functions of the coral skeleton microbiome. *Microbiome*, *7*(1), 159. https://doi.org/10.1186/s40168-019-0762-y

Rickelt, L. F., Lichtenberg, M., Trampe, E. C. L., & Kühl, M. (2016). Fiber-Optic Probes for Small-Scale Measurements of Scalar Irradiance. *Photochemistry and Photobiology*, *92*(2), 331-342. https://doi.org/https://doi.org/10.1111/php.12560

Salih, A., Larkum, A., Cox, G., Kühl, M., & Hoegh-Guldberg, O. (2000). Fluorescent pigments in corals are photoprotective. *Nature*, *408*(6814), 850-853. https://doi.org/10.1038/35048564

Shapiro, O. H., Fernandez, V. I., Garren, M., Guasto, J. S., Debaillon-Vesque, F. P., Kramarsky-Winter, E., Vardi, A., & Stocker, R. (2014). Vortical ciliary flows actively enhance mass transport in reef corals. *Proceedings of the National Academy of Sciences*, *111*(37), 13391-13396. https://doi.org/doi:10.1073/pnas.1323094111

Shashar, N., Cohen, Y., & Loya, Y. (1993). Extreme Diel Fluctuations of Oxygen in Diffusive Boundary Layers Surrounding Stony Corals. *Biol Bull*, *185*(3), 455-461. https://doi.org/10.2307/1542485

Spicer, G. L. C., Eid, A., Wangpraseurt, D., Swain, T. D., Winkelmann, J. A., Yi, J., Kühl, M., Marcelino, L. A., & Backman, V. (2019). Measuring light scattering and absorption in corals with Inverse Spectroscopic Optical Coherence Tomography (ISOCT): a new tool for non-invasive monitoring. *Scientific Reports*, *9*(1), 14148. https://doi.org/10.1038/s41598-019-50658-3

Swain, T. D., DuBois, E., Gomes, A., Stoyneva, V. P., Radosevich, A. J., Henss, J., Wagner, M. E., Derbas, J., Grooms, H. W., Velazquez, E. M., Traub, J., Kennedy, B. J., Grigorescu, A. A., Westneat, M. W., Sanborn, K., Levine, S., Schick, M., Parsons, G., Biggs, B. C., Rogers, J. D., Backman, V., & Marcelino, L. A. (2016). Skeletal light-scattering accelerates bleaching response in reef-building corals. *BMC Ecol*, *16*, 10. https://doi.org/10.1186/s12898-016-0061-4

Taherzadeh, D., Picioreanu, C., & Horn, H. (2012). Mass transfer enhancement in moving biofilm structures. *Biophys J*, *102*(7), 1483-1492. https://doi.org/10.1016/j.bpj.2012.02.033

Tamir, R., Eyal, G., Kramer, N., Laverick, J. H., & Loya, Y. (2019). Light environment drives the shallow-to-mesophotic coral community transition. *Ecosphere*, *10*(9), e02839. https://doi.org/https://doi.org/10.1002/ecs2.2839

Tandon, K., Pasella, M. M., Iha, C., Ricci, F., Hu, J., O'Kelly, C. J., Medina, M., Kühl, M., & Verbruggen, H. (2022). Every refuge has its price: Ostreobium as a model for understanding how algae can live in rock and stay in business. *Semin Cell Dev Biol*. https://doi.org/10.1016/j.semcdb.2022.03.010

Taylor Parkins, S. K., Murthy, S., Picioreanu, C., & Kühl, M. (2021). Multiphysics modelling of photon, mass and heat transfer in coral microenvironments. *Journal of The Royal Society Interface*, *18*(182), 20210532. https://doi.org/10.1098/rsif.2021.0532

Teneva, L., Karnauskas, M., Logan, C. A., Bianucci, L., Currie, J. C., & Kleypas, J. A. (2012). Predicting coral bleaching hotspots: The role of regional variability in thermal stress and potential adaptation rates [Article]. *Coral Reefs*, *31*(1), 1-12. https://doi.org/10.1007/s00338-011-0812-9

Terán, E., Méndez, E. R., Enríquez, S., & Iglesias-Prieto, R. (2010). Multiple light scattering and absorption in reef-building corals. *Applied Optics*, *49*(27), 5032-5042. https://doi.org/10.1364/AO.49.005032

Todd, P. A. (2008). Morphological plasticity in scleractinian corals. *Biol Rev Camb Philos Soc*, *83*(3), 315-337. https://doi.org/10.1111/j.1469-185x.2008.00045.x

van der Zande, R. M., Achlatis, M., Bender-Champ, D., Kubicek, A., Dove, S., & Hoegh-Guldberg, O. (2020). Paradise lost: End-of-century warming and acidification under business-as-usual emissions have severe consequences for symbiotic corals. *Global Change Biology*, *26*(4), 2203-2219. https://doi.org/https://doi.org/10.1111/gcb.14998

Van Woesik, R., Irikawa, A., Anzai, R., & Nakamura, T. (2012). Effects of coral colony morphologies on mass transfer and susceptibility to thermal stress. *Coral Reefs*, *31*(3), 633-639. https://doi.org/10.1007/s00338-012-0911-2

Veal, C. J., Carmi, M., Dishon, G., Sharon, Y., Michael, K., Tchernov, D., Hoegh-Guldberg, O., & Fine, M. (2010). Shallow-water wave lensing in coral reefs: a physical and biological case study. *Journal of Experimental Biology*, *213*(24), 4304-4312. https://doi.org/10.1242/jeb.044941

Wangpraseurt, D., Jacques, S., Lyndby, N., Holm, J. B., Pages, C. F., & Kühl, M. (2018). Microscale light management and inherent optical properties of intact corals studied with optical coherence tomography. *bioRxiv*, 376723. https://doi.org/10.1101/376723

Wangpraseurt, D., Jacques, S. L., Petrie, T., & Kühl, M. (2016). Monte Carlo Modeling of Photon Propagation Reveals Highly Scattering Coral Tissue [Original Research]. *Frontiers in Plant Science*, *7*(1404). https://doi.org/10.3389/fpls.2016.01404

Wangpraseurt, D., Larkum, A., Ralph, P., & Kühl, M. (2012). Light gradients and optical microniches in coral tissues [Original Research]. *Frontiers in Microbiology*, *3*. https://doi.org/10.3389/fmicb.2012.00316

Wangpraseurt, D., Larkum, A. W., Franklin, J., Szabó, M., Ralph, P. J., & Kühl, M. (2014). Lateral light transfer ensures efficient resource distribution in symbiont-bearing corals. *J Exp Biol*, *217*(Pt 4), 489-498. https://doi.org/10.1242/jeb.091116

Wangpraseurt, D., Polerecky, L., Larkum, A. W. D., Ralph, P. J., Nielsen, D. A., Pernice, M., & Kühl, M. (2014). The in situ light microenvironment of corals. *Limnology and Oceanography*, *59*(3), 917-926. https://doi.org/https://doi.org/10.4319/lo.2014.59.3.0917

Wangpraseurt, D., Sun, Y., You, S., Chua, S.-T., Noel, S. K., Willard, H. F., Berry, D. B., Clifford, A. M., Plummer, S., Xiang, Y., Hwang, H. H., Kaandorp, J., Diaz, J. M., La Jeunesse, T. C., Pernice, M., Vignolini, S., Tresguerres, M., & Chen, S. (2022). Bioprinted Living Coral Microenvironments Mimicking Coral-Algal Symbiosis. *Advanced Functional Materials*, *32*(35), 2202273. https://doi.org/https://doi.org/10.1002/adfm.202202273

Wangpraseurt, D., Wentzel, C., Jacques, S. L., Wagner, M., & Kühl, M. (2017). In vivo imaging of coral tissue and skeleton with optical coherence tomography. *Journal of The Royal Society Interface*, *14*. https://doi.org/10.1098/rsif.2016.1003

Wangpraseurt, D., You, S., Azam, F., Jacucci, G., Gaidarenko, O., Hildebrand, M., Kühl, M., Smith, A. G., Davey, M. P., Smith, A., Deheyn, D. D., Chen, S., & Vignolini, S. (2020). Bionic 3D printed corals. *Nature Communications*, *11*(1), 1748. https://doi.org/10.1038/s41467-020-15486-4